Micropumps For Microfluidic Applications

Alexandro Tomassini 40029074, Ian Cesar Ferreira Felix, Zachary Jauniaux 27053487

***Abstract*— A reciprocating diaphragm micropump was designed using arbitrary specifications which closely follow specifications depicted in literature. The construction of the pump is entirely based on silicon due to its favorable mechanical properties. The design was broken into 3 components including a general pump analysis, a diaphragm analysis, and a check valve analysis. A simulated model for the diaphragm and check value was conducted in Simscape to determine the natural frequencies of the components. The final design was modeled in SolidWorks and an overview of the manufacturing process was explored.**

I. Introduction

Microelectromechanical systems (MEMS) are miniature devices which have been manufactured using micromachining techniques developed for the chip manufacturing industry [1]. MEMS devices are comprised of components ranging in size between 1-100 micrometers [2]. These devices can be found in many applications ranging from sensors that measure the flow rate of fluids to accelerometers in cars which determine when to activate airbags. Due to the novelty of this technology coupled with its wide range of possible applications the creation of a new emerging field called microfluidics was achieved [3]. Microfluidics is the study of fluid behavior and manipulation at the microscale. At these small sizes, fluids are heavily affected by surface forces as opposed to volumetric forces [4].

The MEMS device which will be designed is the micropump used for microfluidic applications. Micropumps are used in many fields including biology, medicine, and space exploration. One of the first micropump used was in the early 1980s for the dispensing of insulin [5]. These types of devices were focused on precision measurements over higher volumetric flow rates.

II. Literary Review

According to the literature, micropumps find themselves in two categories. The first category is called the displacement/mechanical type pump and the second category is called the non-mechanical/dynamic pump [5] [6]. The displacement pumps aim to exert pressure forces onto the working fluid through moving parts [5]. The different components which make up a displacement pump include check valves, an oscillating membrane or turbine which function together to move a specific quantity of fluid volume per pump cycle [7]. The dynamic pumps function by continuously increasing the momentum or pressure of a fluid by adding energy into the system [5]. The micropump which has experienced the most amount of research is the reciprocating displacement micropump [5]. This micropump uses a driver to increase or decrease the chamber volume by deforming the pump diaphragm. When the chamber volume is increased, fluid is pulled into the pump chamber by the inlet check valve [5] [7]. During the expansion/suction stroke, the design of the output check valve is such that the valve will remain closed while the inlet valve is opened. When the chamber volume is reduced, the contraction/discharge stroke occurs where the inlet check valve remains closed, and the outlet valve is allowed to open. The fluid will thus leave the pump and the two-stroke pump cycle is completed [5] [7].

III. Design Specification

In order to design a micropump, the desired specifications must be known. Since no specific requirements are known, arbitrary values have been selected by observing several micropump specifications in different research publications [5] and assume the micropump would have similar operational characteristics.

TABLE 1
MICROPUMP DESIGN SPECIFICATIONS

Symbol	Quantity	Value
Q	Volumetric Flow Rate	$1\ \frac{mL}{min}$
f	Diaphragm Operational Frequency	$1000\ Hz$
Δp_{max}	Generated Pressure	$10\ kPa$
v_{fluid}	Fluid Velocity	$0.1\ \frac{m}{s}$

The micropump will be fabricated entirely by silicon due to the silicon's favorable mechanical properties.

TABLE 2
SILICON MECHANICAL PROPERTIES

Symbol	Quantity	Value
ρ	Density	$2330\ \frac{kg}{m^3}$ [8]
ν	Poisson Ratio	0.28 [8]
E	Modulus of Elasticity	112 GPa [9]
σ_y	Yield Strength	120 MPa [9]

The working fluid for the micropump will be water.

TABLE 3
WORKING FLUID PROPERTIES

Symbol	Quantity	Value
κ	Water Compressibility Factor	$45.8e^{-11}\ Pa^{-1}$ [10]

IV. Analysis

A. Pump Analysis

1) Pump Stroke Volume

To determine the stroke volume required to achieve the desired pump specifications, the volumetric flow rate equation (1) will be manipulated.

$$Q = \Delta V * f \text{ [5]} \tag{1}$$

Where Q represents the micropump flowrate in $\frac{m^3}{s}$, f represents the operational frequency in Hz and ΔV represents the change in volume in m^3 which represents the micropump stroke volume. The stroke volume corresponds to the amount of liquid being moved by the pump every cycle.

2) Pump Chamber Volume

To determine the chamber volume of the micropump which represents the pump cavity volume, equation (2) will be manipulated.

$$\Delta p_{max} = \frac{1}{\kappa}\varepsilon_C = \frac{1}{\kappa}\left(\frac{\Delta V}{V_0}\right) \text{ [5]} \tag{2}$$

Where Δp_{max} represents the generated pump pressure in Pa, κ represents the working fluid compressibility factor in Pa^{-1} and ε_C represents the compression ratio. The compression ratio can be expressed by the ratio between the stroke volume and the chamber volume where both volumes are expressed in m^3.

3) Inlet/Outlet Size

To determine the micropump inlet and outlet cross-sectional area, equation (3) will be manipulated. it is important to determine the velocity of the working fluid with respect to the micropumps Compare a specific liquid velocity and compare it to the design specs with regards to the volumetric flow rate.

$$Q = A_{Inlet/Outlet} * v_{fluid} \tag{3}$$

Where Q represents the micropump flowrate in $\frac{m^3}{s}$, v_{fluid} represents the fluid velocity in $\frac{m}{s}$, and $A_{Inlet/Outlet}$ represents the cross-sectional area of the inlet/outlet in m^2.

B. Diaphragm Design

1) Dimension Analysis

a) Flexural Rigidity

Flexural rigidity represents a structures resistance to bending [11]. The flexural rigidity of a diaphragm can be calculated using the following equation:

$$D = \frac{Et^3}{12(1-\nu^2)} \text{ [11]} \tag{4}$$

Where D represents the flexural rigidity in Nm^2, E represents the modulus of elasticity of the material in Pa, t represents the diaphragm thickness in m and ν represents the Poisson's Ratio of the material.

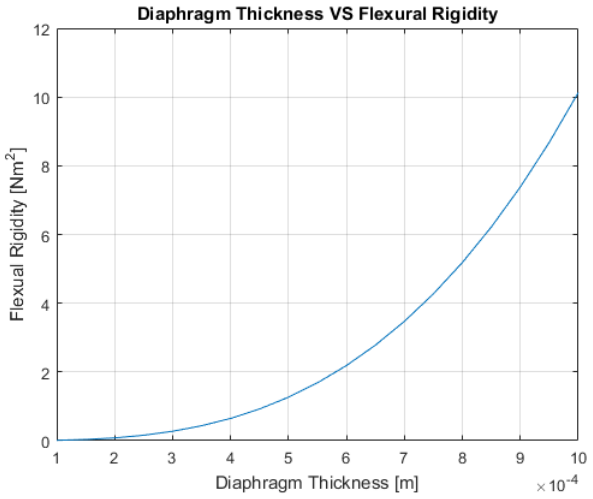

Figure 1. A plot representing a range of diaphragm thicknesses from 100 microns to 1000 microns and their respective flexural rigidity values.

As illustrated in figure 1, the flexural rigidity increases dramatically as the thickness of the diaphragm is increased.

b) Rectangular Plate Deflection

The micropump diaphragm will be simulated as a rectangular plate. The deflection of the plate can be modeled using the following equation:

$$w(x,y) = \frac{q_0}{\pi^4 D}\left(\frac{1}{a^2}+\frac{1}{b^2}\right)^{-2} \sin\left(\frac{\pi x}{a}\right)\sin\left(\frac{\pi y}{b}\right) \text{ [11]} \tag{5}$$

Where $w(x,y)$ represents the diaphragm deflection at the x and y coordinate in m, q_0 represents the actuation pressure present over the entire diaphragm surface in Pa, D represents the flexural rigidity in Nm^2, and a/b represents the edge lengths of the diaphragm.

Since the actuation pressure q_0 is unknown, it is not possible to simulate the diaphragm deflection. In order to solve for the actuation pressure, the area underneath the surface created by equation (5) can be used to determine the actuation pressure. At full actuation, the deflection of the diaphragm will create a volume which represents the stroke volume ΔV of the micropump. Given the stroke volume ΔV required for the micropump is known, the following equation can be used to solve for the actuation pressure q_0:

$$\Delta V = \int_0^a \int_0^b w(x,y)\,dx\,dy$$

$$\Delta V = \int_0^a \int_0^b \frac{q_0}{\pi^4 D}\left(\frac{1}{a^2}+\frac{1}{b^2}\right)^{-2} \sin\left(\frac{\pi x}{a}\right)\sin\left(\frac{\pi y}{b}\right) dx\, dy \qquad (6)$$

By solving equation (6), the actuation pressure q_0 can be determined for any diaphragm design. This is important because for a known stroke volume, many different possible diaphragm dimensions can be modeled as follows:

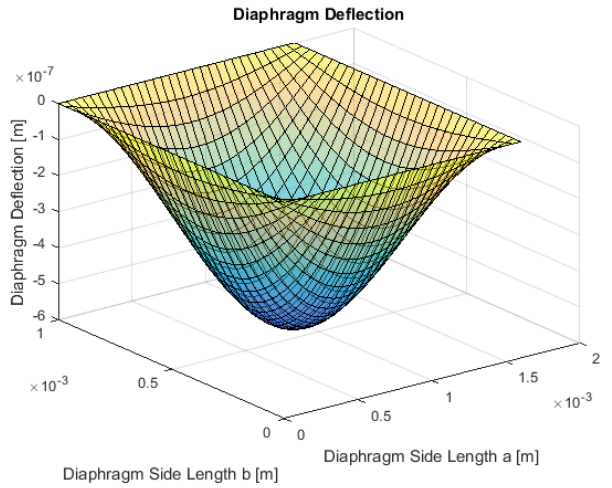

Figure 2. The diaphragm modeled has the following dimensions: Length of side a: 1600 microns, Length side b: 1000 microns, Diaphragm thickness: 100 microns. The largest deflection is 32.72 nm which occurs at the center of the diaphragm. The actuation pressure was calculated as 62.42 kPa.

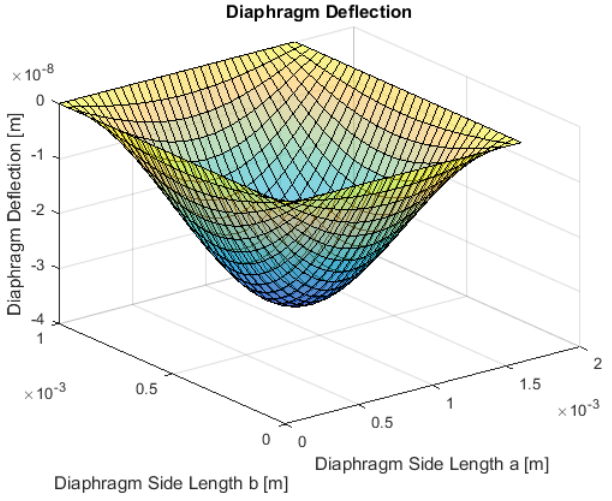

Figure 3. The diaphragm modeled has the following dimensions: Length of side a: 1600 microns, Length side b: 1000 microns, Diaphragm thickness: 1000 microns. The largest deflection is 32.72 nm which occurs at the center of the diaphragm. The actuation pressure was calculated as 10385.89 kPa.

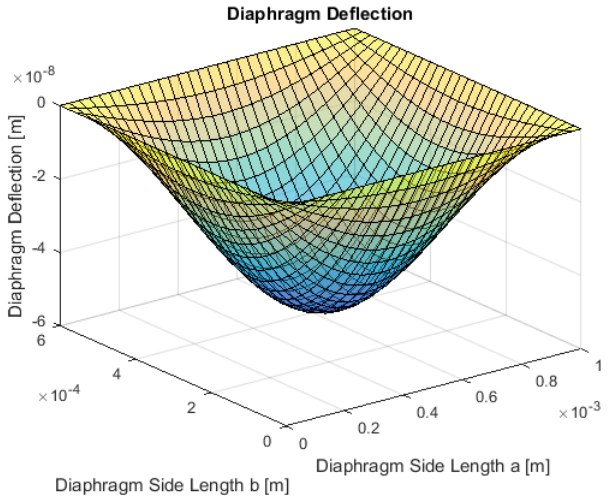

Figure 4. The diaphragm modeled has the following dimensions: Length of side a: 1000 microns, Length side b: 600 microns, Diaphragm thickness: 100 microns. The largest deflection is 52.35 nm which occurs at the center of the diaphragm. The actuation pressure was calculated as 737.14 kPa.

When comparing figure 2 and figure 3, we notice the actuation pressure increases drastically when the diaphragm thickness has been increased. Since both diaphragms have the same edge lengths, the deflection for both models must be the same given the stock volume is held constant. We can deduce that as the diaphragm thickness increases, to achieve the same stoke volume, the actuation pressure must increase to compensate for the increase in flexural rigidity. The opposite would be true when the diaphragm thickness is reduced.

When comparing figure 2 and figure 4, we notice both the max deflection and actuation pressure has increased. Since the diaphragm in figure 4 has been shrunk and its edge lengths are smaller than the edge lengths for the diaphragm in figure 2, we notice the diaphragm deflection must increase to match the desired stroke volume. In order to achieve this larger deflection, the actuation pressure must increase even though the diaphragm thickness is constant between both figures. The opposite would occur if the edge lengths were to increase.

2) Diaphragm Stresses

When designing the micropump, it is important to ensure the diaphragm will not fail during operation. During operation, the diaphragm will be subjected to an actuation pressure which will induce stresses in the diaphragm structure. Two sets of equations will be used to calculate the stresses experienced by the diaphragm. Equations (7) and (8) will determine the stresses at the center of the diaphragm, while equation (9) will determine the max stress experienced by diaphragm which occurs on the middle edge of the longest side of the diaphragm.

$$\sigma_x = -\frac{12Dz}{H^3}\left(\frac{\partial^2 w}{\partial x^2}+\nu\frac{\partial^2 w}{\partial y^2}\right)\,[11]\,[12] \qquad (7)$$

$$\sigma_y = -\frac{12Dz}{H^3}\left(\nu\frac{\partial^2 w}{\partial x^2}+\frac{\partial^2 w}{\partial y^2}\right)\,[11]\,[12] \qquad (8)$$

Where $\sigma_{x/y}$ represents the center stress along the respective direction in Pa, D represents the flexural rigidity in Nm^2, z represents the distance from the neutral axis of the diaphragm in m, H represents the diaphragm thickness in m, and ν represents the Poisson's Ratio.

$$\sigma_{max} = \frac{pb^2}{2t^2\left[0.623\left(\frac{b}{a}\right)^6 + 1\right]} \text{[13]} \quad (9)$$

Where σ_{max} represent the maximum stress experienced by the diaphragm in Pa, t represents the diaphragm thickness in m, p represents the actuation pressure in Pa, b represents the length of the shortest side and a represents the length of the longest side.

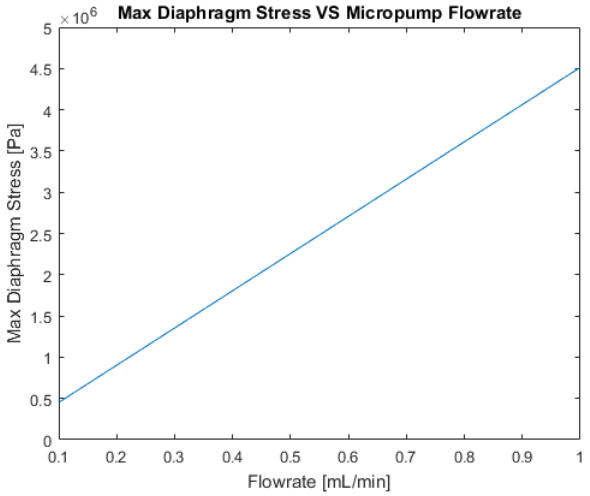

Figure 5. Consequences of altering the micropump flowrate while the operational frequency remains constant at 1000 Hz. The diaphragm being modeled has the following dimensions: Length of side a: 1600 microns, Length side b: 1000 microns and diaphragm thickness: 100 microns.

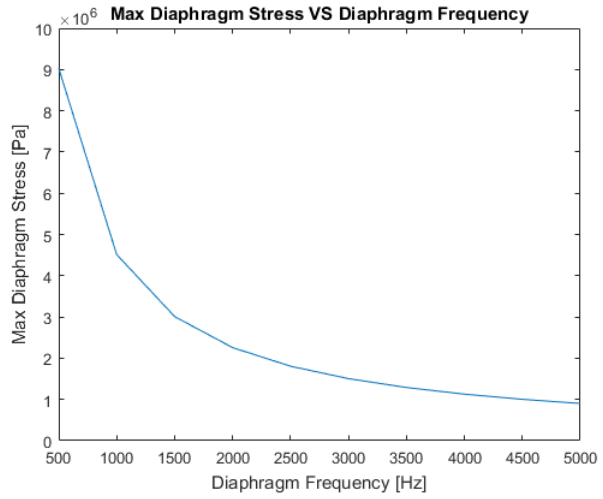

Figure 6. Consequences of altering the micropump operational frequency while the flowrate remains constant at 1 $\frac{mL}{\text{min}}$. The diaphragm being modeled has the following dimensions: Length of side a: 1600 microns, Length side b: 1000 microns and diaphragm thickness: 100 microns.

Figures 5 and 6 illustrate interesting properties for the micropump design. When altering either the flowrate or the operational frequency, the stroke volume will be altered as observed in equation (1). In the case of figure 5, by increasing the flowrate of the micropump, the stroke volume will also need to increase. This means the actuation pressure will have to increase given the diaphragm must deform a larger amount. By increasing the actuation pressure, in turn the maximum diaphragm stress will also increase. The opposite relationship occurs when looking at figure 6. By increasing the number of stroke cycles to achieve a desired flowrate, the stroke volume can decrease because the decreased volume will be compensated by additional strokes. Due to the decreased stroke volume, the actuation pressure will also decrease because the diaphragm deflection will be smaller and thus the maximum stress experienced will also decrease. It is important to make sure the diaphragm operational frequency is kept below the diaphragm natural frequency when adjusting the design to accommodate for design stresses to not exceed the yield strength of the silicon material.

C. Check Valve Design

1) Dimension Analysis

a) Moment of Inertia

The check valves for the micropump will be modeled as cantilever beams. To determine the moment of inertia for a cantilever beam, the following equation will be used:

$$I = \frac{bh^3}{12} \text{[14]} \quad (10)$$

Where I represents the moment of inertia in m^4, b represents the beam width in m, and h represents the beam height in m.

Since the cantilever beam dimensions are unknown, a range of possible dimensions have been modelled in Matlab and plotted in figure 7. The beam width ranges from a minimum width representing the inlet/outlet width plus a 10-micron offset to an upper limit representing the minimum width plus a 200-micron offset. The minimum beam width is required to make sure the inlet and outlet do not leak during operation. The beam height ranges from 50 microns to 250 microns. As illustrated in figure 7, the moment of inertia increases drastically as the beam height parameter is increased.

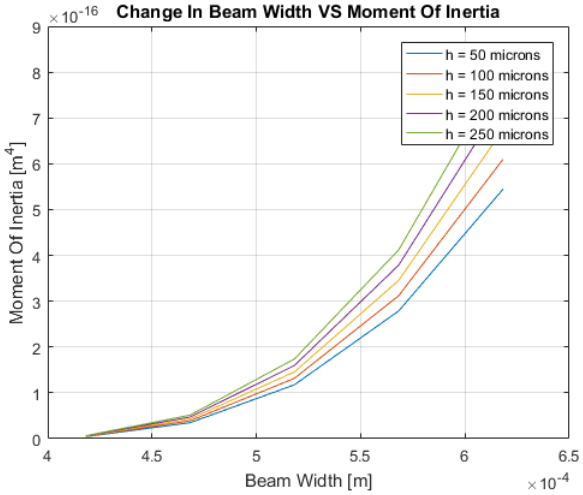

Figure 7. Consequences of altering the cantilever beam width and height. The beam width ranges from 418.2483 μm to 618.2483 μm and the beam height ranges from 50 μm to 250 μm.

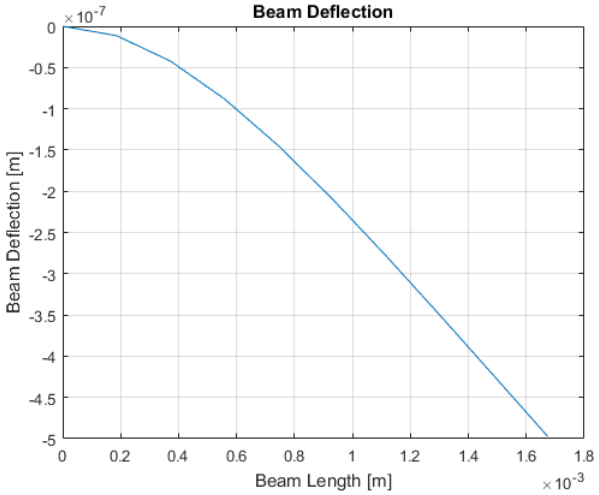

Figure 8. The deflection of a cantilever beam has been modelled. The cantilever beam being modeled has the following dimensions: Beam width: 618.2483 μm, Beam height: 100 μm, Beam length: 1134.8433 μm. The max deflection of the beam is 497.3807 nm.

b) Cantilever Beam Natural frequency

To determine the cantilever beam length, the natural frequency for a cantilever beam will be manipulated using the following equation:

$$f_{CB} = 0.56\sqrt{\frac{EI}{w_{mass}L^4}}\ [15]\ [16] \tag{11}$$

Where f_{CB} represents the cantilever beam natural frequency in Hz, E represents the modulus of elasticity of cantilever beam material in Pa, I represents the moment of inertia in m^4, w_{mass} represents the mass per unit length for the cantilever beam in $\frac{kg}{m}$, and L represents the cantilever beam length in m.

Given the operational frequency of the micropump was determined to be 1000 Hz, this means the check valves will operate at 1000 Hz. Using the rule of 10s, the natural frequency for the cantilever beam will be at least 10 times higher than the operational frequency.

2) Cantilever Deflection

To determine the deflection of the cantilever beam with a distributed load, the following equation will be used to model a cantilever beam:

$$y = \frac{w_{load}}{EI}\left(\frac{-x^4}{24} + \frac{L^3x}{6} - \frac{L^4}{8}\right)\ [17] \tag{12}$$

Where y represents the beam deflection in m, w_{load} represents the distributed load in $\frac{N}{m}$, E represents the modulus of elasticity of the cantilever beam material in Pa, I represents the moment of inertia in m^4, L represents the length of the beam in m, and x represents the distance from the free end of the beam (when $x = 0$, the maximum deflection is present).

3) Beam max stress

When designing the cantilever beam, it is important to ensure the beam does not fail during operation. During operation, the cantilever beam will be subjected to a generated pressure caused by the diaphragm which will induce stresses in the beam when the check valve is activated. To determine the maximum stress induced in cantilever beam, the following equations will be used:

$$M_{max}(at\ fixed\ end) = \frac{w_{load}L^2}{3}\ [18] \tag{13}$$

Where M_{max} represents the maximum moment induced on the cantilever beam in Nm, w_{load} represents the distributed load over the beam in $\frac{N}{m}$, and L represents the cantilever beam length in m.

$$\sigma_{\max stress} = \frac{z*M_{max}}{I}\ [18] \tag{14}$$

Where $\sigma_{\max stress}$ represents the maximum stress experienced by the cantilever beam in Pa, z represents the distance from the neutral axis in m, M_{max} represents the maximum moment induced on the cantilever beam in Nm, and I represents the moment of inertia in m^4.

V. Simulation Models

1) Mass-Spring Simulation

It is possible to simulate the response of a cantilever beam corresponding to the valve and the motion of the diaphragm as a mass-spring system. From the geometry of the parts, one can calculate the volume of the parts that when multiplied by their respective density, the mass is obtained. The constant of the spring is identified by using Hook's law. Simscape was the software selected to simulate the behavior of the valve and diaphragm.

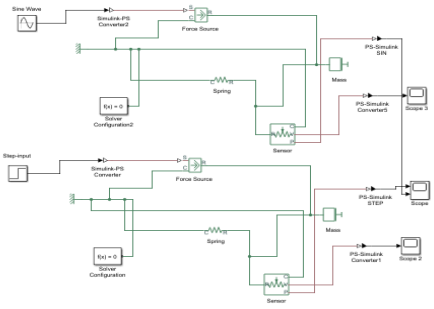

Figure 9. Schematics of the mass-spring system used for the simulation.

By setting the data to the corresponding places it becomes possible to simulate the maximum and minimum displacements of the system, the velocity, and frequencies.

Valve

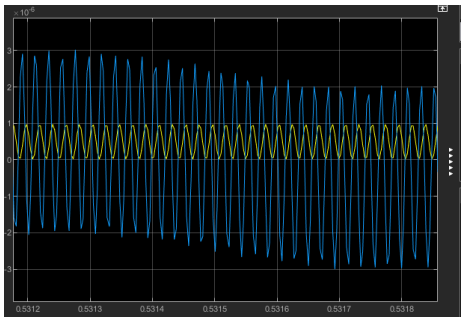

(A)

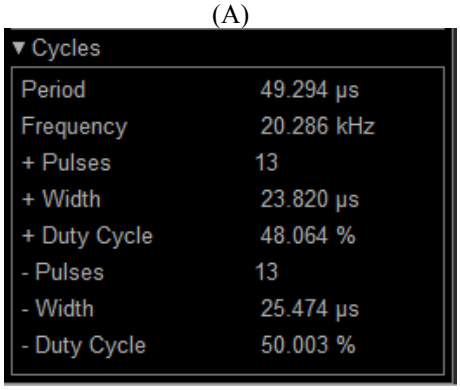

(B)

Figures 10 (A) (B). (A) shows the displacement under a step input in blue and under a sine wave force in yellow. (B) shows the data related to the cycles of the natural frequency of the valve

Diaphragm

The simulation in Simscape yield the following results for the diaphragm:

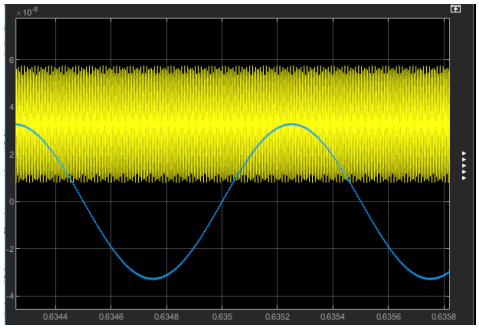

(A)

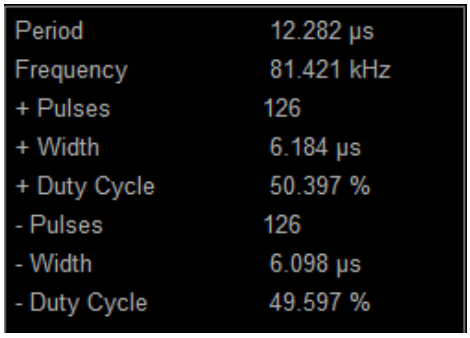

(B)

Figures 11 (A) (B). (A) shows the displacement under a step input and under a sine wave input. (B) shows the data related to the cycles of the natural frequency of the diaphragm.

2) Explanation of the Simulated Results

From the results of the simulation above, it is possible to observe that the system under a sine wave input, will oscillate beyond its natural frequency boundary, generating an oscillation within the already oscillating system. Since the position of the mass is defined by two different frequencies (natural frequency and input frequencies), the overall frequency of the system will vary over time. The step input force on the other hand, will provoke the system oscillate within a constant boundary, as one may notice from the function in yellow.

It should be noticed on the simulations above that the natural frequency does not exactly match those established by design. This happens because the mass-spring system set up in the last section is an attempt to approximate the diaphragm and valves, which are elongated bodies, as point mass systems. The result of this approximation is the discrepancy between the design values and the simulated values.

3) Mathematical Model

It is possible to attempt to model the valve and the diaphragm as a mass spring-system, and as such, they would be described by the differential equation:

$$m\ddot{x} + kx = p(t) \text{ [20]} \quad (18)$$

From the equation (I), m is the mass of the system, k is the spring constant and p(t) is the force applied.
This equation can be rearranged to yield the following equation:

$$\ddot{x} + \frac{k}{m}x = \frac{p(t)}{m} \text{ [20]} \quad (19)$$

Since k/m = ωn^2, the final format of this equation becomes:

$$\ddot{x} + \omega_n^2 x = \frac{p(t)}{m} \text{ [20]} \quad (20)$$

By setting a particular solution for this differential equation, in which p = Psin(ωt) is the force applied and the particular solution x=Xsin(ωt), it becomes possible to observe how the system will respond to different input frequencies by using the following equation:

$$X = \frac{P}{m(\omega_n^2 - \omega^2)} \text{ [20]} \quad (21)$$

In the equation above, P is the amplitude of the force applied, and X is the amplitude of the position of the mass. The increment in the frequency of the systems will yield the following results:

Diaphragm

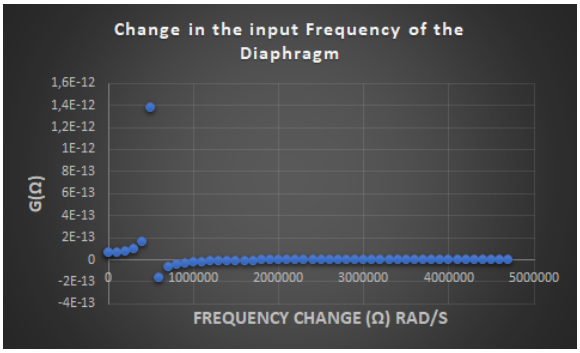

Figure 13. Change in the amplitude of position of the diaphragm as function of frequency

Valve

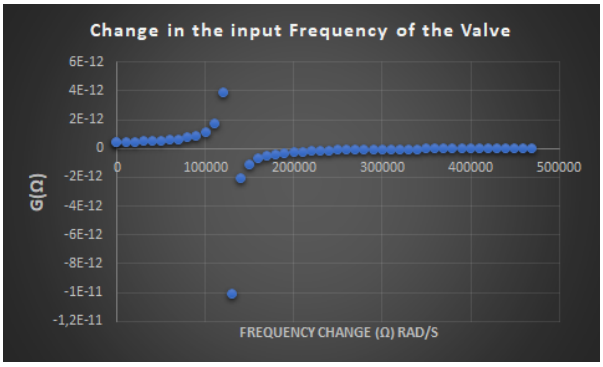

Figure 14. Change in the amplitude of position of the valves as function of frequency

From the two graphs above, it is possible to observe that as the frequencies increase the values X= G(Ω) are very small and increase very little. As the input frequencies approaches to the natural frequency, G(Ω) grows much larger trending towards plus infinity. As the input frequency just surpass the natural frequency, G(Ω) now trends to negative infinity. Finally, as the input frequency continues to grow much larger than the natural frequency, G(Ω) approaches zero, giving the graphs the shapes observed above.

It should be noted that the natural frequencies used in figures 13 and 14 are different from the designed one of 10 KHz. This discrepancy happens because it was attempted to model the valves and the diaphragm and the valves, as mass-spring systems. Both systems do not necessarily behave as point mass systems, and due to this reason, there are going to be differences in the behavior of the simulation and the designed values.

VI. Final Design

TABLE 4
MICROPUMP DESIGN DIMENSIONS

Measure	Value
Chamber Volume	3.639 mL = 3639 mm^3
Stroke Volume	16.67 nL
Inlet/Outlet Area	166666.66 μm^2
Inlet/Outlet Side Length	408.2483 μm
Diaphragm Side Length a	1600 μm
Diaphragm Side Length b	1000 μm
Diaphragm Thickness	100 μm
Diaphragm Max Deflection	32.72 nm
Cantilever Beam Length	1134.8433 μm
Cantilever Beam Width	618.2483 μm
Cantilever Beam Height	100 μm
Cantilever Beam Max Deflection	497.3807 nm

TABLE 5
CALCULATED DIAPHRAGM STRESSES

Measure	Value
σ_x	0.65802 MPa
σ_y	1.0885 MPa
$\sigma_{\max stress}$	3.0095 MPa

TABLE 6
CALCULATED CANTILEVER STRESS

Measure	Value
$\sigma_{\max stress}$	4.877 MPa

Multiple different possible micropump dimension have been simulated in MATLAB. The micropump chamber volume, stroke volume and inlet/outlet area are all dependent on the desired micropump specifications listed in table 1. This means, by changing the desired flowrate, operational frequency, fluid velocity and/or the desired generated pressure, the chamber volume, the stroke volume, and the inlet/outlet size will change as well. If the working fluid used in the micropump was altered, the chamber volume of the micropump would change as well.

The diaphragm dimensions have been selected from a range of modelled dimensions. When examining the stresses in the diaphragm in table 5, it is possible to see that the stresses are far below the yield strength for silicon. This indicates the dimension for the diaphragm has room to be reduced if desired

or the diaphragm thickness can be increased while taking into consideration the required actuation pressure.

With regards to the cantilever beam dimensions, the beam with the largest deflection was selected. Originally, 25 different dimension configurations have been modelled where the desired cantilever beam natural frequency was designed such that the natural frequency occurs at 10 kHz where the natural frequency is 10 times larger than the operational frequency. At 10 kHz, the preferred beam dimension had a length 3588.6897 μm. To reduce the length of the beam, the desired natural frequency was increased to 100 kHz where the beam length was reduced to 1134.8433 μm which is 3 times smaller. 100 kHz is 100 times higher than the operational frequency which is acceptable because it gives the cantilever beam a larger buffer zone before the natural frequency is hit which would cause the micropump to not function correctly. When selecting beam dimensions, it was important to ensure the length and width of the cantilever beam is larger and longer than the inlet/outlet to ensure the micropump is fully sealed during operation. When examining the maximum cantilever beam stress in table 6, it is possible to notice that the maximum stress is drastically lower than the yield stress for silicon.

VII. Fabrication and Modelling

The proposed micropump was designed to be manufactured using 5 stackable Silicon wafers that are individually fabricated through bulk micromachining and wet etching in aqueous KOH. The full model is composed of three major chip components: the valve unit, the chamber unit, and the actuation unit. The three chip components are all made from Silicon wafers of {100} orientation and are bonded through the process of direct wafer bonding [24].

1) Valve Unit

The valve unit consists of 2 identical Silicon wafers that are fabricated through lithography and anisotropic wet etching on both sides of the wafer as seen in Figure 14. The wafers used to create the valve chips have a standard diameter of 3 inches with a thickness of 375μm [24]. Once both wafers have been micromachined, the valve unit is created by bonding the valve wafers together through eutectic bonding [25]. This is a one-step working process that aligns the borders of both wafers and bonds them to create the valve chip unit, as seen in Figure 15.

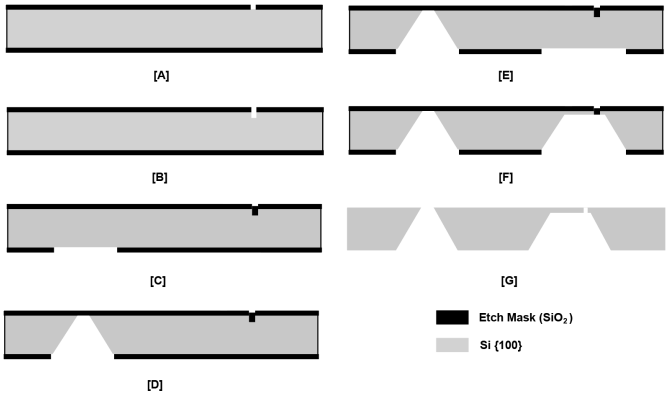

Figure 15. Two-dimensional representation of manufacturing the cantilever check valves using lithography and time constrained anisotropic etching on both sides of an Si wafer: [A] Deposition of etch mask on both sides as well as patterning the top side of the wafer, [B] Etching of top side, [C] Re-deposition of mask on top side and patterning on bottom side, [D] Wet anisotropic etching of through hole that will serve the inlet for the valve, [E] Patterning of bottom side, [F] Time controlled wet etching to create outlet and release the cantilever beam, [G] Removing masks on both sides of the wafer.

It is important to use the front to back alignment method when patterning both sides of a wafer before anisotropic wet etching as seen in Figure 15 [24].

Figure 16. Two-dimensional representation of valve unit after eutectic bonding.

A SolidWorks simulation was conducted on the cantilever beam:

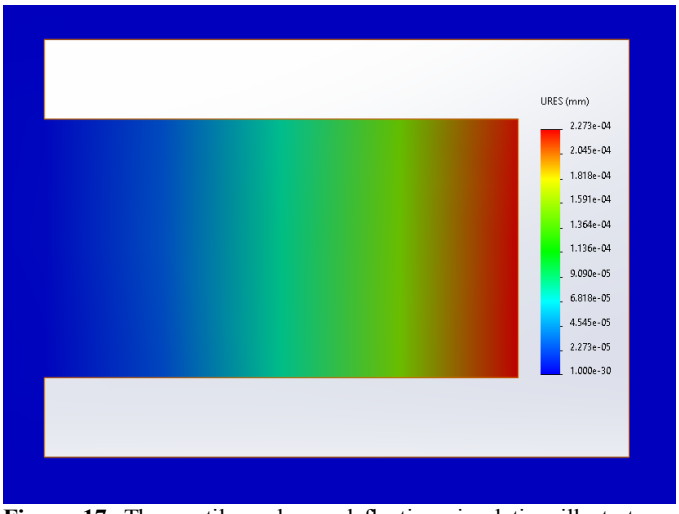

Figure 17. The cantilever beam deflection simulation illustrates a maximum deflection of 227.3 nm which occurs at the free end of the beam.

When comparing the simulated values for deflection with the theoretical values calculated in Matlab, it is possible to notice that the simulated values are less than the theoretical values.

The simulated deflection value is 227.3 nm while the theoretical value is 497.3807 nm.

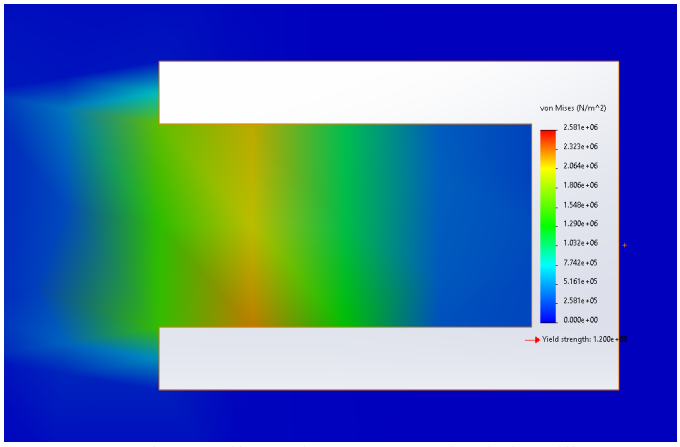

Figure 18. The cantilever beam stress simulation illustrates a maximum stress of 2.581 MPa occurs at the fixed end of the beam.

When comparing the simulated value for the maximum stress with the theoretical values calculated in Matlab, it is possible to notice that the simulated values are less than the theoretical values. The maximum simulated stress value is 2.581 MPa while the maximum theoretical value is 4.877 MPa.

2) Chamber Unit

The chamber unit is manufactured from a non-standard thicker Silicon wafer seeing as the chamber volume needs to be relatively large. Rather than micromachining several different standard wafers, the chamber would be made from a 3inch wafer that has a thickness of 3mm [26]. The wafer is then manufactured as shown in Figure 16. The chamber unit could also potentially be manufactured from Pyrex glass and bonded between the diaphragm unit and the valve unit. This would reduce the cost of manufacturing. This could be an option for an alternative design.

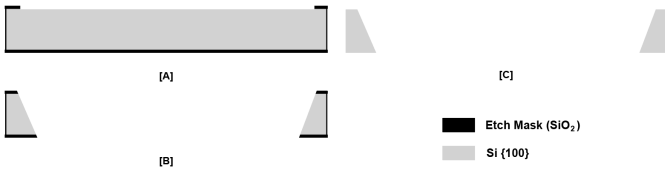

Figure 19. Two-dimensional representation of manufacturing the chamber unit through lithography and anisotropic wet etching: [A] Deposition of etch mask and patterning of top side, [B] Wet anisotropic etching of through hole, [C] Removing etch mask.

3) Actuation Unit

The actuation unit is composed of two, standard 3-inch wafers of thickness 375μm, that are individually micromachined and then bonded together. Unlike the valve unit, the 2 wafers that form the actuation unit aren't identical. The bottom half of the unit includes the pump diaphragm, while the top half of the unit is the counter-electrode that will produce the electrostatic forces that induce the pump stroke [23].

a) Diaphragm

From the design specifications, the pump diaphragm is a rectangular freestanding silicon structure. This kind of structure only requires one lithography step and can be micromachined using time controlled wet anisotropic etching as shown in Figure 20.

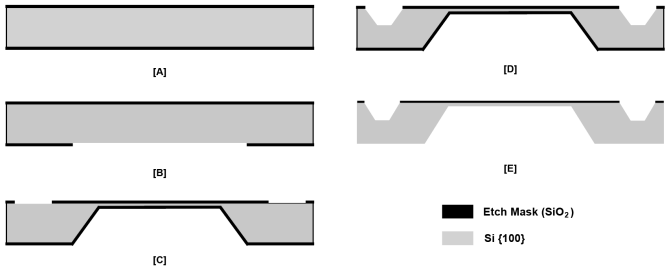

Figure 20. Two-dimensional representation of manufacturing of the bottom half of the actuation unit, which includes the pump diaphragm: [A] Deposition of etch mask on both sides of the wafer, [B] Patterning of bottom side, [C] Time controlled wet anisotropic etching to create desired diaphragm thickness 100μm, patterning top-side as well as re-deposition of etch mask on bottom side [D] Time controlled etching of trenches in top-side of the wafer, [E] Removing mask on bottom-side, top side mask will serve as an isolation layer within the assembly of the actuation unit.

b) Counter Electrode

From the design specifications, the counter electrode was designed in relation to the size of the diaphragm unit.

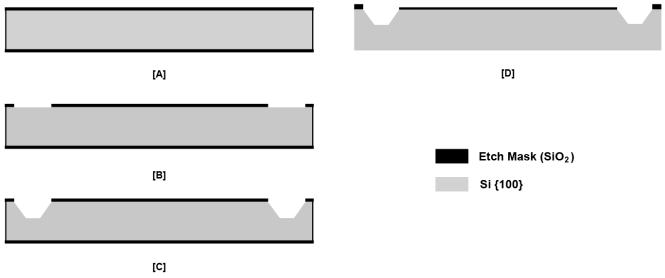

Figure 21. Two-dimensional representation of manufacturing the counter electrode chip: [A] Deposition of etch mask, [B] Patterning, lithography, [C] Time controlled anisotropic wet etching of counter-electrode trenches, [D] Etch mask is kept on one side of the chip as an isolation layer.

Once both the diaphragm chip and the counter-electrode chip have been fabricated, they are assembled together through the working process of anodic bonding [23]. A two-dimensional representation of the actuation unit can be observed in Figure 22.

Figure 22. Two-dimensional representation of actuation unit after anodic bonding.

The actuation gap between the diaphragm and the counter-electrode as seen in Figure 22, is created by sputtering a layer of Pyrex through a shadow mask [23]. The sputtering is used to create a separation of $5\mu m$.

A SolidWorks simulation was conducted on the diaphragm:

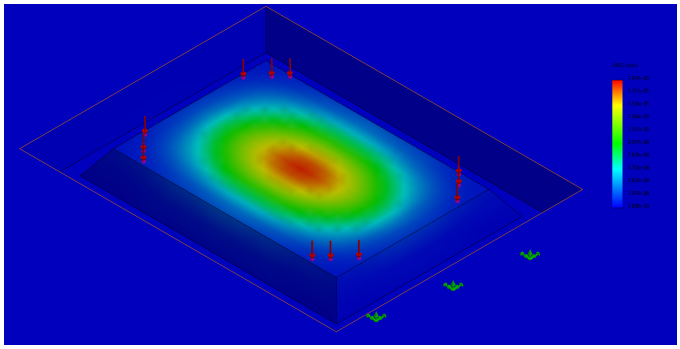

Figure 23. The diaphragm deflection simulation illustrates a maximum deflection of 19.19 nm which occurs at the center of the diaphragm.

When comparing the simulated values for deflection with the theoretical values calculated in Matlab, it is possible to notice that the simulated values are less than the theoretical values. The simulated deflection value is 19.19 nm while the theoretical value is 32.72 nm.

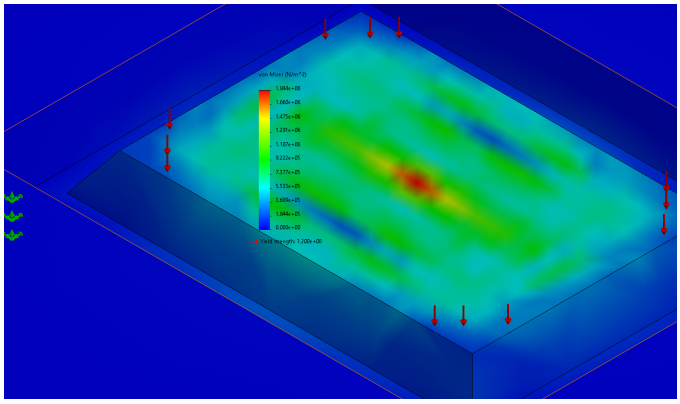

Figure 24. The diaphragm stress simulation illustrates a maximum stress of 1.844 MPa.

When comparing the simulated value for the maximum stress with the theoretical values calculated in Matlab, it is possible to notice that the simulated values are less than the theoretical values. The maximum simulated stress value is 1.844 MPa while the maximum theoretical value is 3.0095 MPa.

4) Micropump Assembly and Modelling

From the designated *Final Design* specifications shown in Table 4, a three-dimensional micropump was modelled in SolidWorks to show a prototype of the final design. The complete assembly can be observed in Figure 25.

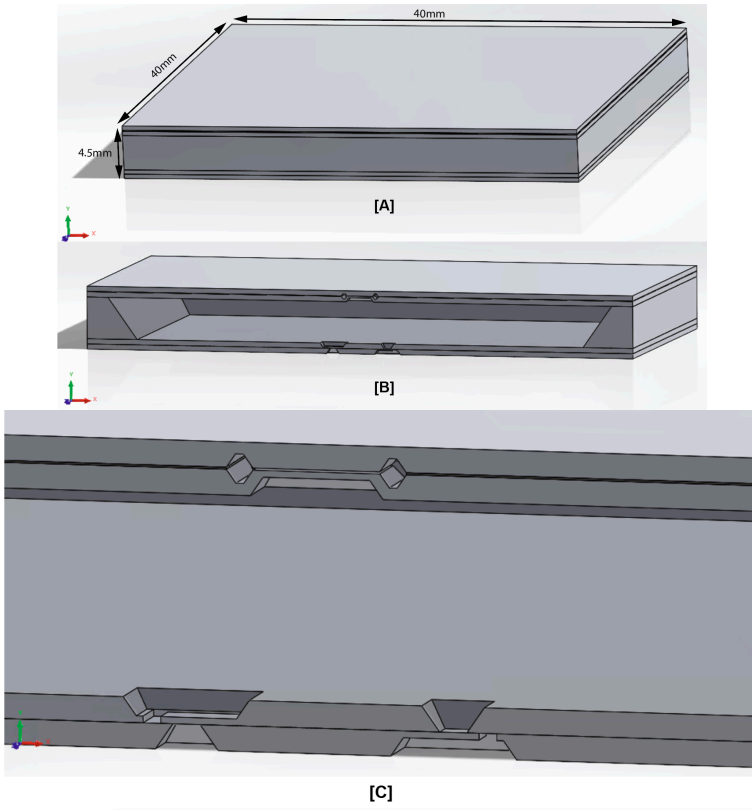

Figure 25. Three-dimensional model of the final Micropump design in SolidWorks: [A] Isometric view of Complete Chip Design and dimensions, [B] Sectional view of the full assembly, [C] Closer sectional view to observe the micromachined components within the design model.

VIII. Conclusion

A reciprocating diaphragm micropump design has been developed which theoretically functions to the desired specifications listed in table 1. The micropump specifications follow closely the values depicted in literature [5]. Simulations, calculations and software models also seem to corroborate that the design will work under the correct frequency and will not fail under stress. For future work, the feasibility of operating this Micropump using Electrostatic forces would need to be further investigated.

IX. References

[1] N. Maluf, An Introduction to Microelectromechanical Systems Engineering, Artech House Print on Demand, 2000.

[2] K. Gabriel, J. Jarvis and W. Trimme, "Small Machines, Large Opportunities: A Report on the Emerging Field of Microdynamics : Report of the Workshop on Microelectromechanical Systems Research," AT & T Bell Laboratories, 1988.

[3] A. Nisar, N. Afzulpurkar, B. Mahaisavariya and A. Tuantranont, "MEMS-based micropumps in drug delivery and biomedical applications," *Sensors and Actuators,* pp. 917-942, 2007.

[4] P. Tabeling and S. Chen, Introduction to Microfluidics, Oxford University Press, 2006.

[5] D. J. Laser and J. G. Santiago, "A review of micropumps," *Micromechanics and microengineering,* pp. 35-64, 2004.

[6] Y.-N. Wang and L.-M. Fu, "Micropumps and biomedical applications – A review," *Microelectronic Engineering,* vol. 195, pp. 121-138, 2018.

[7] N.-T. Nguyen, X. Huang and T. K. Chuan, "MEMS-micropumps: A review," *Journal of Fluids Engineering,* pp. 384-392, 2002.

[8] INSACO, "Silicon," [Online]. Available: https://www.insaco.com/materials/other-materials/silicon. [Accessed 20 Feb 2021].

[9] Solidworks, *Material Properties.*

[10] "Compressibility of Liquids," [Online]. Available: http://hyperphysics.phy-astr.gsu.edu/hbase/Tables/compress.html. [Accessed Feb 2021].

[11] R. D. Cook, Concepts and Applications of Finite Element Analysis, Wiley, 2001.

[12] D. L. Logan, Finite Element Method.

[13] Engineers Edge, "Uniform Load Rectangular Plate Clamped (Empirical) Equations and Calculator," [Online]. Available: https://www.engineersedge.com/material_science/uniform_load_rectangular_plate__13644.htm.

[14] D. Kataria, S. Kumar, S. Balguvhar and R. Mukhiya, "Realization of MEMS-based silicon cantilever using bulk micromachining," 2017.

[15] E. Toolbox, "Beams Natural Vibration Frequency," 2017. [Online]. Available: https://www.engineeringtoolbox.com/structures-vibration-frequency-d_1989.html. [Accessed 2021].

[16] S. İkizoğlu and A. Ö. Ertanır, "Design considerations of a MEMS cantilever beam switch for pull-in under electrostatic force generated by means of vibrations," *JVE Journals,* 2014.

[17] C. Michael, *Deflection of Cantilever Beam For Uniformly Distributed Load,* 2016.

[18] Sandra, "Maximum Deflection Of Fixed Beam With Udl," 2020. [Online]. Available: https://www.cannondigi.com/maximum-deflection-of-fixed-beam-with-udl/.

[19] J. W. C. M. S. K. Y.-E. Y. D.-S. C. Jae Sung Yoon, "Studies on the performance characteristics and improvements of the," *Microelectronic Engineering,* pp. 2300-2303, 18 June 2018.

[20] B. H. Tongue, Principles of Vibration, Berkeley: Oxford University Press, 2002, pp. 4-79.

[21] R. Zengerle, J. Ulrich, S. Kluge, M. Richter and A. Richter, "A Bidirectional Silicon Micropump," *Sensors And Actuators,* pp. 81-86, 1995.

[22] S. A. F. F. Yazdi, A. Corigliano and R. Ardito, "3-D Design and Simulation of a Piezoelectric Micropump," *Micromachines,* vol. 10, no. 4, 2019.

[23] R. Znegerle, H. Sandmaier and A. Richter, "A micromembrane pump with electrostatic actuation," *Fraunhofer Institute for solid state technology,* pp. 19-24, March 1992.

[24] P. Pal and K. Sato, Silicon wet bulk Micromachining for MEMS, Singapore: Pan Stanford Publishing, 2017.

[25] M. Koch, N. Harris, A. G. R. Evans, N. M. White and A. Brunnschweiler, "A novel micropump design with thick-film piezoelectric actuation," *University of Southhampton,* pp. 49-57, 20 September 1996.

[26] "University Wafer," [Online]. Available: https://www.universitywafer.com/thick-silicon-wafers.html. [Accessed 5 march 2021].